


Universal Barenco quantum gates via a tunable noncollinear interaction

Xiao-Feng Shi*

School of Physics and Optoelectronic Engineering, Xidian University, Xi'an 710071, China

 (Received 26 September 2017; revised manuscript received 2 October 2017; published 12 March 2018)

The Barenco gate (\mathbb{B}) is a type of two-qubit quantum gate based on which alone universal quantum computation can be achieved. Each \mathbb{B} is characterized by three angles (α , θ , and ϕ), though it works in a two-qubit Hilbert space. Here we design \mathbb{B} via a noncollinear interaction $V|r_1r_2\rangle\langle r_1r_3| + \text{H.c.}$, where $|r_i\rangle$ is a state that can be excited from a qubit state and V is adjustable. We present two protocols for \mathbb{B} . The first (second) protocol consists of two (six) pulses and one (two) wait period(s), where the former causes rotations between qubit states and excited states, and the latter induces gate transformation via the noncollinear interaction. In the first protocol, the variable ϕ can be tuned by varying the phases of external controls, and the other two variables α and θ , tunable via adjustment of the wait duration, have a linear dependence on each other. Meanwhile, the first protocol can give rise to CNOT and controlled-Y gates. In the second protocol, α , θ , and ϕ can be varied by changing the interaction amplitudes and wait durations, and the latter two are dependent on α nonlinearly. Both protocols can also lead to another universal gate when $\{\alpha, \phi\} = \{1/4, 1/2\}\pi$ with appropriate parameters. Implementation of these universal gates is analyzed based on the van der Waals interaction of neutral Rydberg atoms.

DOI: [10.1103/PhysRevA.97.032310](https://doi.org/10.1103/PhysRevA.97.032310)

I. INTRODUCTION

Data processing in computers involves many gate operations, which is also the case for quantum computation, although the latter works in fundamentally different ways. The information processing in quantum computing can be understood as a series of unitary operations on a given input state [1,2]. If a set of quantum gates can represent an arbitrary unitary operation, it is a universal set [3]. Study of universal sets of quantum gates has been a focus for decades [4–14]. A popular universal set consists of the controlled-NOT (CNOT) gate and either a collection of three fixed-angle single-qubit gates or another collection of four single-qubit gates [2]. In other words, to build a reliable quantum computer requires the preparation of multiple gates of four or five types, each with an adequate accuracy. In 1995, Adriano Barenco introduced the two-qubit quantum gate [4]

$$\mathbb{B} = \begin{pmatrix} 1 & 0 & 0 & 0 \\ 0 & 1 & 0 & 0 \\ 0 & 0 & e^{i\alpha} \cos \theta & -ie^{i(\alpha-\phi)} \sin \theta \\ 0 & 0 & -ie^{i(\alpha+\phi)} \sin \theta & e^{i\alpha} \cos \theta \end{pmatrix}, \quad (1)$$

which by itself constitutes a universal set, where α , θ , and ϕ are fixed irrational multiples of π and of each other. Another universal gate similar to \mathbb{B} was found in Ref. [5]. According to [4], being able to accurately realize \mathbb{B} is sufficient for the construction of a quantum computation network. Since it is challenging to experimentally realize all quantum gates in a universal set with a high accuracy, it seems a more attractive route to build a quantum computer by designing only one gate such as \mathbb{B} , compared with the strategy of designing several single-qubit gates and a CNOT gate.

Although a single two-qubit gate as a universal set was proposed more than two decades ago [4,5], its implementation remains an outstanding challenge. For the case of the Barenco gate, this is possibly because \mathbb{B} has three angles $\{\alpha, \theta, \phi\}$, although it operates on two qubits. Thus designing a CNOT gate (which is usually more challenging than realizing single-qubit gates) is the first choice [15] with systems such as single photons [16], electrons in silicons [17], superconducting circuits [18,19], atomic ions [20], and neutral Rydberg atoms [21,22].

Here we propose two protocols (I and II) for Barenco gates when there is a noncollinear interaction between states that can be excited from the qubit states. Protocol I consists of two π pulses and one wait period, illustrated in Fig. 1, where ϕ is tunable by adjustment of the phases of external control, and α and θ change linearly with the wait duration in different ways. Protocol II consists of six π pulses and two wait periods; α changes linearly with the wait durations, while the other two variables depend on α nonlinearly. Protocol I can lead to CNOT and controlled-Y gates and can be easily tuned to the parameter regime of $\{\alpha, \phi\} = \{1/4, 1/2\}\pi$ and θ being an irrational multiple of π , where \mathbb{B} becomes

$$\mathbb{B}_1 = \begin{pmatrix} 1 & 0 & 0 & 0 \\ 0 & 1 & 0 & 0 \\ 0 & 0 & e^{i\pi/4} \cos \theta & -ie^{-i\pi/4} \sin \theta \\ 0 & 0 & ie^{-i\pi/4} \sin \theta & e^{i\pi/4} \cos \theta \end{pmatrix}, \quad (2)$$

which, being similar to the universal gate introduced in [5], also constitutes a universal set by itself [4]. Protocol II can also realize Eq. (2) if specific interactions are available.

Below, we detail the sequences for the two gate protocols and analyze the experimental prospects of realizing \mathbb{B} by using van der Waals interaction (vdWI) of Rydberg atoms [23]. Before proceeding, we introduce a generic method to construct a noncollinear interaction that is essential to our protocols.

*shixiaofeng@xidian.edu.cn

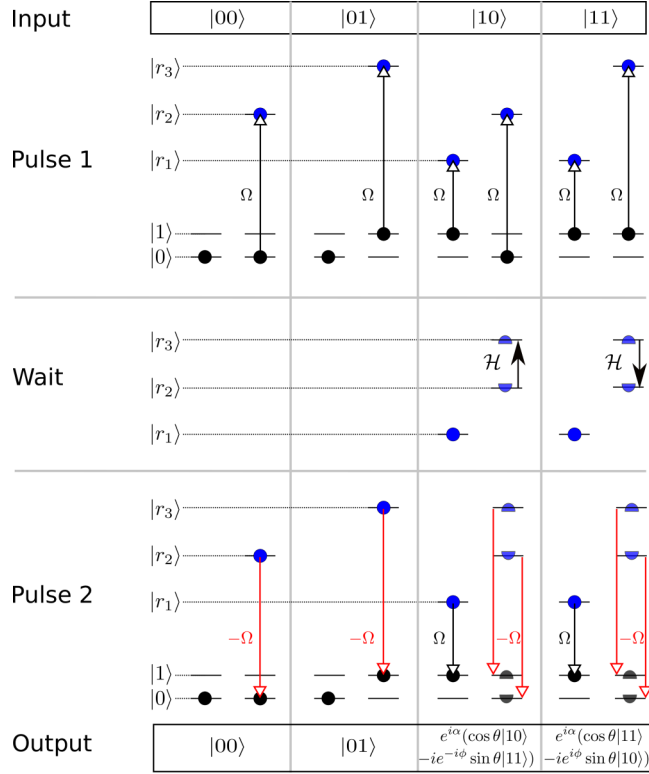


FIG. 1. Protocol I for the Barenco gate. The first pulse maps qubit states to excited states, then the wait period allows the noncollinear interaction to induce state transformation that is essential for the gate, and the second pulse maps the excited states back to qubit states. There is a π phase difference in the external fields between the first and the second pulses on the target qubit.

II. TUNABLE NONCOLLINEAR INTERACTION

Our protocols are based on a noncollinear interaction between states that can be transformed from the qubit states via external control fields, which we introduce here. We denote the basis states of Eq. (1) $\{|00\rangle, |01\rangle, |10\rangle, |11\rangle\}$, where $|\mu\nu\rangle \equiv |\mu\rangle_c \otimes |\nu\rangle_t$ is a two-qubit product state, with $|\mu(\nu)\rangle = |0\rangle$ or $|1\rangle$ being the ground state of a quantum system, and the subscripts c and t denote control and target, respectively. We suppose that no interaction exists in the four computational basis states of the gate. Among the four single-qubit states of the control and target, three can be connected to other states during the gate sequence,

$$|1\rangle_c \leftrightarrow |r_1\rangle_c, \quad |0\rangle_t \leftrightarrow |r_{2(3)}\rangle_t, \quad |1\rangle_t \leftrightarrow |r_{3(2)}\rangle_t,$$

where the kets on the right-hand sides of the double arrows (\leftrightarrow) are either excited states or other ground states that can be connected with the qubit states $|0(1)\rangle$ via external control. In our gate sequence, the input states $|10\rangle$ and $|11\rangle$ can be excited to two states, $|r_1r_2\rangle$ and $|r_1r_3\rangle$, in which the following engineered two-body interaction arises:

$$\mathcal{H} = \begin{pmatrix} V_1 & V_e e^{-i\beta_0} \\ V_e e^{i\beta_0} & V_2 \end{pmatrix}, \quad (3)$$

which is written with the ordered basis $\{|r_1r_2\rangle, |r_1r_3\rangle\}$, where β_0 , V_1 , V_2 , and V_e are real variables. The off-diagonal interaction in Eq. (3) is essential for our method.

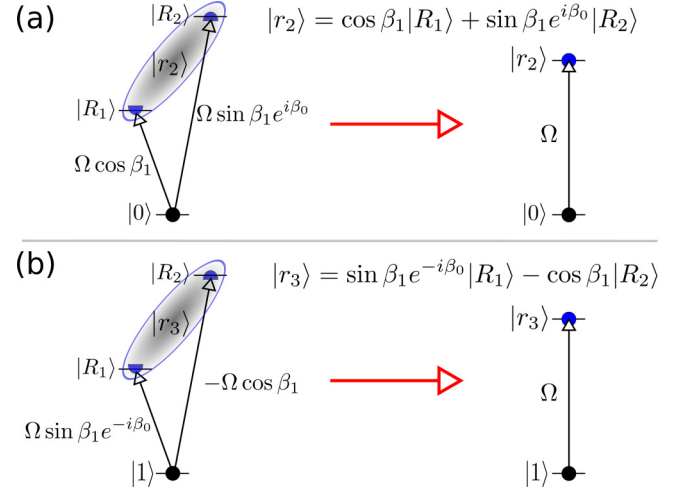


FIG. 2. Excitation of the superposition states in Eq. (5) during pulse 1 of Protocol I. (a) and (b) show the preparation of $|r_2\rangle$ and $|r_3\rangle$, respectively. Different superpositions in $|r_2\rangle$ and $|r_3\rangle$ follow after the different ratios of the two Rabi frequencies on the energy eigenstates $|R_1\rangle$ and $|R_2\rangle$. β_1 is tunable by adjustment of the ratio between the strengths of the laser fields on the two Rydberg eigenstates.

The form of Eq. (3) is a little unusual compared with the more familiar two-body interaction of the form

$$\mathcal{H}_0 = \sum_{j,k=0}^2 b_{jk} |R_j R_k\rangle \langle R_j R_k|, \quad (4)$$

where the energy eigenstates $|R_0\rangle, |R_1\rangle$, and $|R_2\rangle$ are orthogonal to each other, and b_{jk} is a blockade energy shift. Equation (4) can be found in various systems suitable for quantum computing, including (but not limited to) electrons in quantum dots [24], superconducting circuits [25], and neutral Rydberg atoms [26]. Nevertheless, a noncollinear interaction in Eq. (3) rarely appears in qubits for quantum information processing, although it can be found in collective excitations in condensed matter systems [27,28].

To realize Eq. (3) based on Eq. (4), we consider the orthogonal states

$$\begin{aligned} |r_1\rangle &= |R_0\rangle, \quad |r_2\rangle = \cos \beta_1 |R_1\rangle + \sin \beta_1 e^{i\beta_0} |R_2\rangle, \\ |r_3\rangle &= \sin \beta_1 e^{-i\beta_0} |R_1\rangle - \cos \beta_1 |R_2\rangle \end{aligned} \quad (5)$$

in a rotating frame, $\hat{H} \rightarrow e^{i\hat{R}t} \hat{H} e^{-i\hat{R}t} - \hat{R}$, where $\hat{R} = \sum_j E_j |j\rangle \langle j|$ sums over all involved atomic states $|j\rangle$. In this rotating frame, states $|r_2\rangle$ and $|r_3\rangle$ become eigenstates with any mixing angle $\beta_1 \in [0, \pi/2]$. Note that the superposition states above can also be written as

$$\begin{aligned} |r_2\rangle &= e^{i\beta_0} (\cos \beta_1 |R_1\rangle + \sin \beta_1 |R_2\rangle), \\ |r_3\rangle &= \sin \beta_1 |R_1\rangle - \cos \beta_1 |R_2\rangle \end{aligned}$$

by redefining $|R_{1(2)}\rangle$, since a relative phase between $|R_1\rangle$ and $|R_2\rangle$ in $|r_{2(3)}\rangle$ is trivial in our case. $|r_2\rangle$ and $|r_3\rangle$ can be prepared by simultaneously exciting the two excited states $|R_1\rangle$ and $|R_2\rangle$ from the qubit state, shown in Fig. 2. A specific angle β_0 in Eq. (5) is determined by adjusting the phase of the external field on the component $|R_{1(2)}\rangle$ to be $\beta_0(\beta_0 - \pi)$ in $|r_2\rangle$ relative to that in $|r_3\rangle$, as shown in Fig. 2. Take neutral

atoms, for example; $|0(1)\rangle$ is a hyperfine ground state, and $|R_1\rangle$ and $|R_2\rangle$ can be Rydberg eigenstates. When two laser beams of different frequencies are simultaneously delivered to one atom of initial state $|0\rangle$, with one laser exciting $|R_1\rangle$ at Rabi frequency $\Omega \cos \beta_1$ and the other one pumping $|R_2\rangle$ at Rabi frequency $\Omega \sin \beta_1 e^{i\beta_0}$, shown in Fig. 2(a), a rotation between $|0\rangle$ and $|r_2\rangle$ at Rabi frequency Ω is established. Similarly, setting the two Rabi frequencies on $|R_1\rangle$ and $|R_2\rangle$ to $\Omega \sin \beta_1 e^{-i\beta_0}$ and $-\Omega \cos \beta_1$ establishes the preparation of $|r_3\rangle$.

According to Eq. (4), the interaction between the two orthogonal states $|r_1 r_2\rangle$ and $|r_1 r_3\rangle$ can be represented by Eq. (3), where

$$\begin{aligned} V_1 &= b_{01} \cos^2 \beta_1 + b_{02} \sin^2 \beta_1, \\ V_2 &= b_{01} \sin^2 \beta_1 + b_{02} \cos^2 \beta_1, \\ V_e &= (b_{01} - b_{02}) \sin \beta_1 \cos \beta_1. \end{aligned} \quad (6)$$

As long as $b_{01} \neq b_{02}$, V_e can be nonzero. Note that in Eq. (5), we can use $|R_1\rangle$ or $|R_2\rangle$ instead of $|R_0\rangle$ in $|r_1\rangle$. However, when an external control can simultaneously influence both qubits, it is necessary to choose $|r_1\rangle$ to be orthogonal to $|r_{2(3)}\rangle$. The three interaction strengths V_1 , V_2 , and V_e can be tuned by varying β_1 , and the ratio b_{01}/b_{02} is adjustable by choosing different sets of states $\{|R_0\rangle, |R_1\rangle, |R_2\rangle\}$.

Below we present two protocols based on Eq. (3), where the three variables α , θ , and ϕ exhibit distinct tunabilities that can be beneficial for different purposes in quantum control.

III. PROTOCOL I: A TWO-PULSE SEQUENCE

We first show a two-pulse sequence for \mathbb{B} when $V_1 = V_2$ and β_0 in Eq. (3) is tunable. When $|R_j\rangle$ is a state of neutral atoms, where $j = 0-2$, β_0 can be tuned by varying the relative phases among the external control fields.

As illustrated in Fig. 1, Protocol I starts with a π pulse of Rabi frequencies Ω on the control and target qubit states $|1\rangle_c$, $|0\rangle_t$, and $|1\rangle_t$,

$$\{|1\rangle_c, |0\rangle_t, |1\rangle_t\} \mapsto -i\{|r_1\rangle_c, |r_2\rangle_t, |r_3\rangle_t\}. \quad (7)$$

When $\Omega \gg \{V_1, V_2, V_e\}$, we have the following map:

$$\{|00\rangle, |01\rangle, |10\rangle, |11\rangle\} \mapsto -\{i|0r_2\rangle, i|0r_3\rangle, |r_1r_2\rangle, |r_1r_3\rangle\}.$$

The process above is subject to a residue blockade effect which can be minimized by increasing Ω relative to $V_{1(2)}$ and V_e .

Upon completion of pulse 1, a wait period of duration T is allowed when the two-atom state evolves under the interaction in Eq. (3):

$$\begin{aligned} |r_1 r_2\rangle &\mapsto \eta_1 e^{-iT\lambda_+} |\lambda_+\rangle + \eta_2 e^{-iT\lambda_- + i\beta_0} |\lambda_-\rangle, \\ |r_1 r_3\rangle &\mapsto \eta_2 e^{-iT\lambda_+ - i\beta_0} |\lambda_+\rangle - \eta_1 e^{-iT\lambda_-} |\lambda_-\rangle. \end{aligned} \quad (8)$$

Here

$$\begin{aligned} \lambda_{\pm} &= (V_1 + V_2)/2 \pm \bar{V}, \\ |\lambda_+\rangle &= \eta_1 |r_1 r_2\rangle + \eta_2 e^{i\beta_0} |r_1 r_3\rangle, \\ |\lambda_-\rangle &= \eta_2 e^{-i\beta_0} |r_1 r_2\rangle - \eta_1 |r_1 r_3\rangle \end{aligned}$$

are the eigenvalues and normalized eigenvectors of Eq. (3), where $\bar{V} = \sqrt{V_e^2 + (V_1 - V_2)^2/4}$ and $\eta_1 : \eta_2 = V_e : (2\bar{V} +$

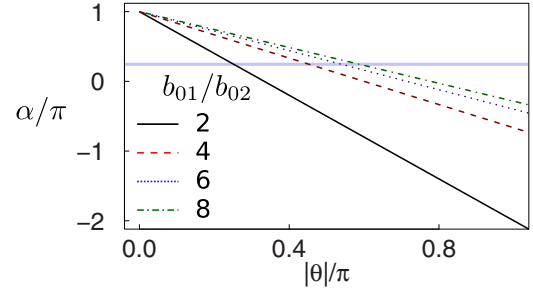


FIG. 3. α as a function of $|\theta|$ in Protocol I for the \mathbb{B} gate with several values of b_{01}/b_{02} . θ is positive (negative) if $b_{01} - b_{02} > 0$ ($b_{01} - b_{02} < 0$). The other variable ϕ in the gate is freely tunable. The horizontal gray line locates $\alpha = \pi/4$, a value that satisfies the condition for another universal gate when $\phi = \pi/2$ and b_{01}/b_{02} is irrational [4].

$V_2 - V_1)/2$. For the sake of convenience, a frequently appearing Planck constant is hidden.

Soon after the wait period, another set of external fields with strengths similar to those in the first pulse is applied, with a π phase shift in the control fields on the target qubit. The Rabi frequency on the control is still Ω , but those on the target become $-\Omega$, so as to induce the map

$$\{|r_1\rangle_c, |r_2\rangle_t, |r_3\rangle_t\} \mapsto i\{-|1\rangle_c, |0\rangle_t, |1\rangle_t\}, \quad (9)$$

which differs from Eq. (7) in that the phase change to a state of the target qubit is $\mp\pi/2$ in Eq. (7) [Eq. (9)].

As can be easily verified, the state evolution from input to output under the condition of $V_1 = V_2$ [or, equivalently, $\beta_1 = \pm\pi/4$ in Eq. (6)] is

$$\begin{aligned} |00\rangle &\mapsto |00\rangle, \\ |01\rangle &\mapsto |01\rangle, \\ |10\rangle &\mapsto e^{i\alpha} (-ie^{-i\phi} \sin \theta |11\rangle + \cos \theta |10\rangle), \\ |11\rangle &\mapsto e^{i\alpha} (\cos \theta |11\rangle - ie^{i\phi} \sin \theta |10\rangle). \end{aligned} \quad (10)$$

Here

$$\begin{aligned} \alpha &= \pi - V_1 T = \pi - (b_{01} + b_{02})T/2, \\ \theta &= V_e T = \pm |b_{01} - b_{02}|T/2, \\ \phi &= -\beta_0, \end{aligned} \quad (11)$$

where $+$ ($-$) in θ applies for a positive (negative) V_e . Equation (10) is exactly gate \mathbb{B} in Eq. (1). Here ϕ is determined by phases of external control fields and, thus, is tunable and independent of $\{\alpha, \theta\}$. α and θ depend on the wait duration and the interaction strengths b_{01} and b_{02} and have a linear relation with each other:

$$\alpha = \pi - \frac{b_{01} + b_{02}}{b_{01} - b_{02}} \theta. \quad (12)$$

When $b_{01} - b_{02} > 0$, α is shown in Fig. 3 as a function of θ with several sets of b_{01}/b_{02} . As proven in Ref. [4], Eq. (10) is a useful Barenco gate when α , θ , and ϕ are irrational multiples of π and of each other. In the above protocol, θ can be tuned by choosing an appropriate T to be any irrational multiple of π , and simultaneously α is an irrational multiple of π at least for a rational b_{01}/b_{02} , according to Eq. (12). Finally, ϕ can

be tuned to any value via variation of the relative phases of external fields. So, there should be infinite sets of α , θ , and ϕ that are irrational multiples of π and of each other.

From Ref. [4], when $\{\alpha, \phi\} = \{1/4, 1/2\}\pi$ and θ is an irrational multiple of π , the gate in Eq. (10) also constitutes a universal set. Equation (12) indicates that θ is an irrational multiple of π when b_{01}/b_{02} is irrational and $\alpha = \pi/4$. Since the condition of $\alpha = \pi/4$ is readily achievable as indicated by the horizontal line in Fig. 3, and b_{01}/b_{02} in a real system can be an irrational number infinitely near a rational b_{01}/b_{02} such as those in Fig. 3, Protocol I can construct the universal gate in Eq. (2) in addition to the Barenco gate.

A. CNOT and controlled-Y gates

Below, we show that Protocol I can also lead to CNOT and control-Y gates. Although such gates cannot constitute a universal set unless single-qubit rotations are brought in, realization of an “overcomplete” family of universal gates may be helpful to construct a quantum computing circuit [2]. Meanwhile, though a single quantum gate as a universal set has certain advantages such as a lower overhead in calibration, it can be less efficient for certain quantum computation algorithms. In principle, single-qubit rotations together with any two-qubit entangling gate can build up a quantum computing network, and an entangling gate which is less challenging to realize is often the favorite of current interest, which is why the CNOT gate has received widespread attention.

Protocol I can easily lead to a CNOT gate. As seen from Eq. (11), when $b_{01} > 0$ and $b_{02} = 0$, a wait time $T = \pi/b_{01}$ in Protocol I leads to $\alpha = \theta = \pi/2$. Setting $\beta_0 = 0$ ensures $\phi = 0$; then the gate transformation of Protocol I in Eq. (10) becomes

$$\begin{aligned} |00\rangle &\mapsto |00\rangle, & |01\rangle &\mapsto |01\rangle, \\ |10\rangle &\mapsto |11\rangle, & |11\rangle &\mapsto |10\rangle \end{aligned} \quad (13)$$

as in a CNOT gate. The requirement for this CNOT gate can be easily set for neutral atoms. First, the condition $b_{01} > 0$ is fulfilled by choosing both $|r_1\rangle$ and $|R_1\rangle$ in Eq. (5) from a common high-lying s -orbital Rydberg state $|R_0\rangle$. Take $|r_1\rangle = |R_1\rangle = |96s_{1/2}, m_J = 1/2, m_I = 3/2\rangle$ as an example; the calculated [29] interaction coefficient $b_{01} = 36 \times 2\pi$ THz $(\mu\text{m}/l)^6$ is about $0.6 \times 2\pi$ MHz even when the two qubits are separated by the large distance of $l = 20 \mu\text{m}$.

The other requirement for realizing a CNOT gate, $b_{02} = 0$, is achievable by choosing $|R_2\rangle$ from a ground state, since the interaction between Rydberg and ground states can be neglected. Specifically, if $|0(1)\rangle = |5s_{1/2}, F = 1(2), m_F = -1\rangle$, one can choose $|R_2\rangle$ as $|5s_{1/2}, F = 1, m_F = 1\rangle$, a state that can be reached from both $|0\rangle$ and $|1\rangle$ by using detuned circularly polarized laser fields on an intermediate state, $|5p_{1/2}, F = 1, m_F = 0\rangle$. Take $|0\rangle \rightarrow |r_2\rangle$, for example; its excitation is shown in Fig. 4, with its effective Rabi frequency Ω given by $\Omega_1\Omega_2/\sqrt{2}\Delta$ [29]. Because circularly polarized laser fields induce transitions between two levels differing in hyperfine quantum numbers by $\Delta m_F = \pm 1$, the laser connecting $|5p_{1/2}, F = 1, m_F = 0\rangle$ and $|R_2\rangle$ in Fig. 4 may also couple $|0(1)\rangle$ leftward to a level with $m_F = -2$. Such a coupling, however, is negligible via the selected $|5p_{1/2}, F = 1\rangle$ manifold because it does not host a state with $m_F = -2$. Similarly,

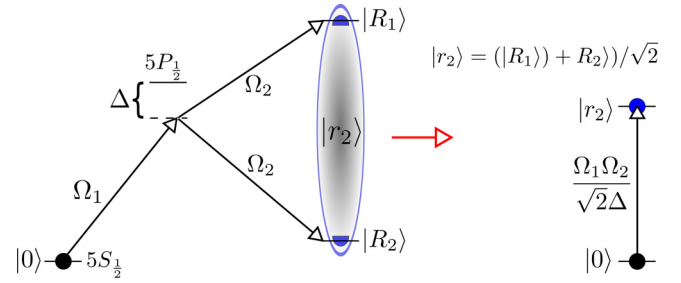


FIG. 4. Scheme for constructing $|r_2\rangle$ so that $b_{02} = 0$ in Eq. (6) for realizing CNOT and control-Y gates. Here Δ is a detuning that is large compared with Ω_1 and Ω_2 . A similar configuration for $|r_3\rangle$ is realized when the two Rabi frequencies on $|R_1\rangle$ and $|R_2\rangle$ are Ω_2 and $-\Omega_2$.

the laser addressing $|0(1)\rangle \leftrightarrow |5p_{1/2}, F = 1, m_F = 0\rangle$ in Fig. 4 cannot couple $|R_2\rangle$ with $|5p_{1/2}, F = 1\rangle$ since it does not host a state with $m_F = 2$. Alternatively, level shifting by a strong enough external magnetic field can be applied to avoid population leakage if we use a coupling scheme different from that in Fig. 4.

Protocol I can also realize the controlled-Y gate. Still, we use a similar setting described above to reach the domain of $b_{01} > 0$ and $b_{02} = 0$ so that $\alpha = \theta = \pi/2$ can be achieved by choosing a wait duration of $T = \pi/b_{01}$. Differently from the CNOT gate above, here the phase of the laser field shall render $\beta_0 = -\pi/2$ so that $\phi = \pi/2$. Then Eq. (10) shows that the gate maps the states according to

$$|10\rangle \mapsto -i|11\rangle, \quad |11\rangle \mapsto i|10\rangle, \quad (14)$$

while the other two input states, $|00\rangle$ and $|01\rangle$, are not affected, realizing the controlled-Y gate.

IV. PROTOCOL II: A SIX-PULSE SEQUENCE

Below, we describe Protocol II, where each of the three angles $\{\alpha, \theta, \phi\}$ depends on model parameters in a manner different from that in Protocol I. The six-pulse protocol below is based on $V_1 \neq V_2$ and $\beta_0 = 0$ in Eq. (3). A six-pulse sequence is chosen so as to show details, although we can also adopt a four-pulse sequence because the first (last) two pulses can occur simultaneously. For the sake of convenience, we use pulse k to denote the k th pulse, where $k = 1-6$.

Pulse 1 is a π pulse on state $|1\rangle_c$ of the control qubit, so that

$$\{|10\rangle, |11\rangle\} \mapsto -i\{|r_1 0\rangle, |r_1 1\rangle\},$$

while the other two states $|00\rangle$ and $|01\rangle$ stay intact.

Pulse 2 is a simultaneous π pulse on qubit states $|0\rangle_t, |1\rangle_t$. When $\Omega \gg \{V_1, V_2, V_e\}$, we have the following map:

$$\{|00\rangle, |01\rangle, -i|r_1 0\rangle, -i|r_1 1\rangle\} \mapsto -\{|0r_2\rangle, i|0r_3\rangle, |r_1 r_2\rangle, |r_1 r_3\rangle\}.$$

Upon completion of pulse 2, a wait period of duration T is allowed when the two-qubit state evolves under the interaction in Eq. (3), where the state evolution is identical to that in Eq. (8), with $\beta_0 = 0$.

Pulse 3 maps the states of the target qubit to the ground states, i.e., inverse to pulse 2:

$$\{|r_2\rangle_t, |r_3\rangle_t\} \mapsto -i\{|0\rangle_t, |1\rangle_t\}.$$

Pulse 4 is also a π pulse but maps the states of the target qubit to excited states in a different manner than pulse 2 does:

$$\{|0\rangle_t, |1\rangle_t\} \mapsto -i\{|r_3\rangle_t, |r_2\rangle_t\}. \quad (15)$$

Upon completion of pulse 4, we again allow a wait period of duration T , so that the four input states $\{|00\rangle, |01\rangle, |10\rangle, |11\rangle\}$ evolve, respectively, to $\{i|0r_3\rangle, i|0r_2\rangle, \chi_1|r_1r_2\rangle + \chi_2|r_1r_3\rangle, \chi_3|r_1r_2\rangle + \chi_4|r_1r_3\rangle\}$, where

$$(\chi_1, \chi_2, \chi_3, \chi_4) = e^{i\alpha} \cos \theta (ie^{-i\phi} \tan \theta, -1, -1, ie^{i\phi} \tan \theta)$$

and

$$\begin{aligned} \alpha &= -T(V_1 + V_2), \\ \sin \theta &= 2(\eta_1 \eta_2) \{(\eta_1^2 - \eta_2^2)^2 [\cos(2T\bar{V}) - 1]^2 \\ &\quad + \sin^2(2T\bar{V})\}^{1/2}, \\ \cos \theta &= 1 + 4\eta_1^2 \eta_2^2 [\cos(2T\bar{V}) - 1], \\ \sin \phi &= 2(\eta_1 \eta_2) (\eta_1^2 - \eta_2^2) [\cos(2T\bar{V}) - 1] / |\sin \theta|, \\ \cos \phi &= 2(\eta_1 \eta_2) \sin(2T\bar{V}) / |\sin \theta|. \end{aligned} \quad (16)$$

Pulse 5 is identical to pulse 4 so as to induce a state transformation inverse to Eq. (15), and finally, pulse 6 is inverse to pulse 1. As a consequence, the overall effect on the four input states is described by Eq. (10), which can be represented in the matrix form of Eq. (1).

Similarly to Protocol I, in Protocol II there are many cases where α , θ , and ϕ are irrational multiples of π and of each other. α , θ , and ϕ are functions of the three variables $V_1 T$, $V_2 T$, and $V_e T$. For each set $\{V_1, V_2, V_e\}$, when T changes, α changes linearly, but θ and ϕ evolve nonlinearly. By choosing several sets of $(V_1 : V_2 : V_e)$, we show in Fig. 5 that θ and ϕ evolve in different ways, indicating the existence of many choices of α , θ , and ϕ that are irrational multiples of π and of each other.

Protocol II also allows realization of \mathbb{B}_1 in Eq. (2). The condition $\{\alpha, \phi\} = \{1/4, 1/2\}\pi$ can be satisfied with $T = \pi/2\bar{V}$ when $V_1 + V_2 = -\bar{V}/2$, where the latter condition requires $-b_{01}/b_{02} = 5/3$ or $3/5$. If one realizes \mathbb{B}_1 by using Rydberg interaction of neutral atoms, the desired b_{01}/b_{02} can be reached either by using external fields to tune the energy gaps between appropriate Rydberg levels or by introducing another independent variable β_2 when choosing a superposition state for $|R_2\rangle$ in Eq. (5),

$$|R_2\rangle \rightarrow \cos \beta_2 |R_2\rangle + \sin \beta_2 |R_3\rangle, \quad (17)$$

so that the parameter b_{02} in Eq. (6) becomes tunable by varying β_2 ,

$$b_{02} \rightarrow b_{02} \cos^2 \beta_2 + b_{03} \sin^2 \beta_2.$$

When $b_{02} < b_{03}$, the scheme above transfers the former b_{02} to a new one tunable in the interval $[b_{02}, b_{03}]$. If Eq. (17) is adopted, it is necessary to use microwave fields that are strong enough to suppress the transition from $\cos \beta_2 |R_2\rangle + \sin \beta_2 |R_3\rangle$ to $(\cos \beta_2 |R_3\rangle - \sin \beta_2 |R_2\rangle)$, as detailed in [30].

V. REALIZATION WITH NEUTRAL ATOMS

We turn to an analysis of the feasibility of realizing the protocols above with two neutral ^{87}Rb atoms. As for the

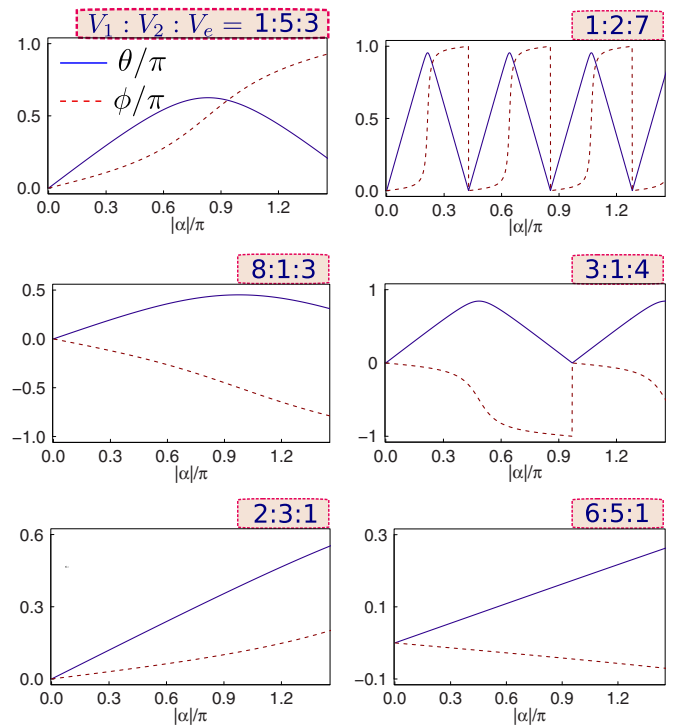


FIG. 5. The two variables θ and ϕ as a function of α in Protocol II for the \mathbb{B} gate. Here we choose six sets of $(V_1 : V_2 : V_e)$, shown above each panel.

qubit states, one can choose from the hyperfine ground states $|0(1)\rangle = |5s_{1/2}, F = 1(2), m_F = 0\rangle$ for both the control and the target [21], where $\{F, m_F\}$ constitute the hyperfine notation of the ground states. For Rydberg states introduced below, however, we apply the fine structure notation according to the spectroscopic resolution achieved in experiments.

The interaction defined in Eqs. (3) and (6) can be from vdWI between neutral atoms, which we briefly introduce here. When each of two nearby neutral atoms is in a Rydberg state $|R_0\rangle$, a strong interaction between the electric dipole moments of the two atoms can arise. When this interaction energy is much smaller than the energy gaps to other nearby two-atom Rydberg states, it causes an overall energy shift b_{00} [see Eq. (4)] to the two-atom Rydberg state [23]. Such vdWI can be several tens of megahertz, which is strong enough to induce fast quantum dynamics on the single-quantum level [31]. This means that when one atom is already in a Rydberg state $|R_0\rangle$, it is difficult to use resonant fields to excite a nearby atom to $|R_0\rangle$ unless the applied field is very strong. Based on this blockade interaction, Ref. [32] proposed two-qubit controlled-phase gates, one of which was experimentally demonstrated years ago [21]. Since then, there have been various proposals of two-qubit controlled-phase (or CNOT) gates based on Rydberg blockade [33]. Instead of focusing on the blockade mechanism, this work relies on the exchange interaction of Rydberg atoms, which has been much less explored either experimentally [34] or theoretically [29,35,36] for the purpose of quantum information processing. The exchange interactions used in [29] and [34–36], however, are limited to the type where the states of both atoms change simultaneously. In contrast, the exchange

process of Eq. (3) in this work only changes the state of the target qubit.

We illustrate the performance of the gate by choosing

$$\begin{aligned} |R_0\rangle &= |R_1\rangle = |n_1 s_{1/2}, m_J = 1/2, m_I = 3/2\rangle, \\ |R_2\rangle &= |n_2 s_{1/2}, m_J = 1/2, m_I = 3/2\rangle \end{aligned} \quad (18)$$

for the construction of $|r_j\rangle$ in Eq. (5), where n_1 and n_2 are two different large principal quantum numbers, and m_J (m_I) denotes the electric (nuclear) spin projection on the quantization axis. Preparation of a superposition Rydberg state $|r_{2(3)}\rangle$ can be performed via two-photon excitation in the V or Y' configuration, as shown in Fig. 2 and detailed in [30] and [37], although here we need not stabilize the superposition by extra external fields unless Eq. (17) is used.

A. Intrinsic fidelity

Regarding the gate fidelity \mathcal{F} [38], the Rydberg state decay, blockade errors from incomplete rotations, and population leakage to levels other than qubit states render imperfect gate operation characterized by a fidelity error $1 - \mathcal{F}$. This error can be estimated from analytical approximations [39]. For example, the decay-induced error can be estimated from the fact that the population loss due to Rydberg state decay is proportional to the time staying in a Rydberg state. We estimate $1 - \mathcal{F}$ by choosing $\{n_1, n_2\} = \{96, 102\}$, a two-atom distance of $20 \mu\text{m}$, a Rabi frequency $\Omega/2\pi = 30 \text{ MHz}$, and an environment temperature of 4 K . The vdWI for this choice is given in Appendix A. We let β_1 be $\pi/4$ and $3\pi/8$ for Protocols I and II, respectively, since β_1 should (should not) be $\pm\pi/4$ for Protocol I (Protocol II): If $|\beta_1| = \pi/4$ in Protocol II, ϕ becomes $0, \pm\pi, \dots$. We show the variables α , θ , and ϕ and the fidelity error rescaled by 10^3 in Fig. 6 for both Protocol I and Protocol II, according to Eqs. (11) and (16) and the estimates in Appendix B. ϕ in Protocol I is not shown in Fig. 6(a) because it is determined by phases of external fields. If we instead assume a temperature of 300 K , a larger error from Rydberg state decay occurs and the fidelity error $1 - \mathcal{F}$ in Fig. 6 increases to be in the interval $[0.7, 5.7]([2.0, 12]) \times 10^{-3}$ for Protocol I (Protocol II). Here two other error-causing factors have been ignored. First, we find that errors from the force between the two atoms when both of them are in Rydberg states can be ignored, as shown in Appendix B. Second, an extra error $\bar{E}_{\mathcal{L}}$ from the position fluctuation of the atoms can be neglected too. To show the smallness of $\bar{E}_{\mathcal{L}}$, we assume optical tweezer traps created by single laser beams with wavelength $\lambda = 1.1 \mu\text{m}$ and waist $w = 3 \mu\text{m}$. If the atoms are not cooled to motional ground states before the gate sequence, numerical calculation as in [30] and [40] shows that $\bar{E}_{\mathcal{L}} \in [1.4, 52]([1.0, 49]) \times 10^{-4}$ for Protocol I (Protocol II) when the effective atomic temperature $T_a \in [10, 200] \mu\text{K}$ and the trap depth is $U = 20 \text{ mK}$. We also considered a similar setup analyzed in Ref. [40], where atoms are cooled to motional ground states, and found that $\bar{E}_{\mathcal{L}} < 7 \times 10^{-5}$ for both Protocol I and Protocol II when $U > 1 \mu\text{K}$. So, the error caused by position fluctuation can be suppressed by sufficient cooling of the atoms.

The gate fidelity in most cases in Fig. 6 is heavily hampered by the decay probability of Rydberg states, which is mainly determined by the wait duration T and thus inversely proportional to the vdWI parameters V_1 , V_2 , and V_e [see Eqs. (11)

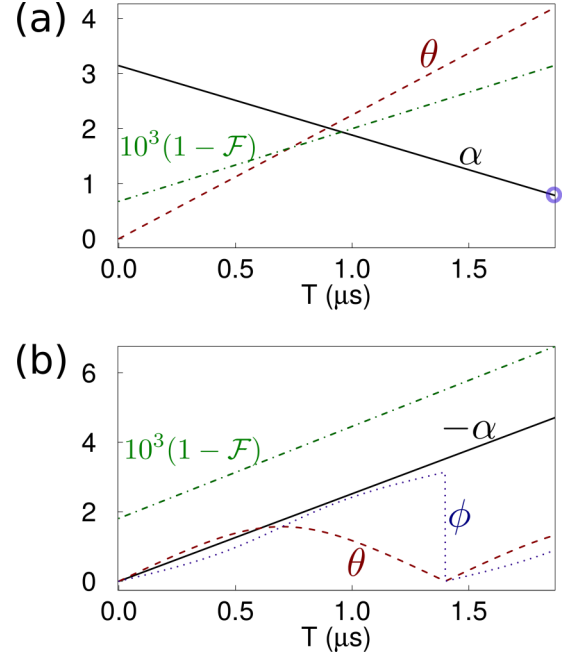


FIG. 6. The solid, dashed, dotted, and dash-dotted curves, respectively, show the three variables α , θ , and ϕ and the total error (scaled up by 10^3) of the intrinsic gate fidelity as a function of T in the \mathbb{B} gate protocols realized with two neutral ^{87}Rb atoms. (a) Protocol I and (b) Protocol II. The circle on the curve of α in (a) locates the value of $\alpha = \pi/4$.

and (16)]. Appendix A shows that V_1 , V_2 , and V_e in Fig. 6 are smaller than $2\pi \text{ MHz}$, resulting in microsecond-scale gate times and significant Rydberg state decay. But if we use larger vdWI by decreasing the qubit spacing, the calculated vdWI can approach the energy gap to nearby two-qubit Rydberg states and violates the picture of vdWI. However, it is possible to tackle this issue via pulse shaping, a technique useful in neutral atoms [41] as well as solid-state systems [42].

In principle, the intrinsic gate fidelity error in Fig. 6 can be significantly suppressed by recently proposed schemes. For example, the blockade error can be removed by exploring rational generalized Rabi frequencies in detuned Rabi transitions [40], and population leakage can be reduced in the adiabatic regime [36]. Our purpose here, however, is to provide simplest protocols for \mathbb{B} so as to inspire further exploration of quantum information processing by using the interaction in Eq. (3).

B. Tunable operation modes

Four parameters are tunable in the two protocols: the frequency, intensity, and phase of the laser fields of optical pulses and the wait duration T between the optical pulses. First, the interaction coefficients b_{jk} can be adjusted by choosing different eigenstates in Eqs. (4) and (18) via using lasers of different frequencies. If the eigenstates $|R_0\rangle$ and $|R_1\rangle$ in Eq. (4) are Rydberg states, but $|R_2\rangle$ is a ground state, then we have the condition $b_{02} = 0$ for the realization of CNOT and controlled-Y gates, as described in Sec. III A. Below, we discuss the tunability when the eigenstates $|R_{j(k)}\rangle$ in Eq. (4) are all Rydberg states.

For every set of $|R_{j(k)}\rangle$ in Eq. (4), the angle β_1 in Eq. (5) can be tuned by adjusting the intensity of the laser fields. For example, when lasers in Fig. 2 are set such that $\beta_1 = k\pi/2$ with an integer k , the noncollinear coefficient V_e disappears in Eq. (3), which is a case where neither Protocol I nor Protocol II leads to a Barenco gate. By continuously changing the magnitudes of the laser fields on the two Rydberg states $|R_{1(2)}\rangle$ in Fig. 2(a) [or Fig. 2(b)], the mixing angle β_1 in the definition of $|r_2\rangle$ [or $|r_3\rangle$] can be continuously changed. When $\beta_1 = \pi/4$, $V_1 = V_2$ is achieved and Protocol I can be realized.

The ratio between V_1 , V_2 , and V_e can be tuned by changing the mixing angle β_1 in Protocol II, so that the scaling of the angles α , θ , and ϕ can behave in distinct ways, shown in Fig. 5. For instance, when $b_{01} \gg b_{02} > 0$, we have $(V_1 : V_2 : V_e) \approx (\cos^2 \beta_1 : \sin^2 \beta_1 : \sin \beta_1 \cos \beta_1)$, which includes at least two cases: $V_1 > V_e > V_2$ and $V_2 > V_e > V_1$. Similarly, if $b_{01} > -b_{02} > 0$, we can realize another pair of cases: $V_e > V_1 > V_2$ and $V_e > V_2 > V_1$. When $b_{01} \sim b_{02} > 0$, adjusting β_1 can lead to $V_1 > V_2 > V_e$ and $V_2 > V_1 > V_e$, covering all cases in Fig. 5.

Furthermore, the angle β_0 in Eq. (5) can be tuned by adjusting the relative phases of laser fields on the two Rydberg states $|R_{1(2)}\rangle$ in Figs. 2(a) and 2(b). This is crucial for Protocol I: although the angles α and θ in Eq. (1) are determined by the wait duration T , the angle ϕ is determined by phases of the laser fields, shown in Eq. (11).

Finally, the wait duration T in both protocols can be varied, so that the angles α and θ in Protocol I and all three angles, α , θ , and ϕ , in Protocol II can be tuned.

In summary, when the frequency, intensity, and phase of the laser fields and the wait duration between laser pulses are tuned, various sets of the three angles in the Barenco gate can be realized.

C. Experimental prospects

High-fidelity realization of the above protocols depends on the availability of strong enough pulsed lasers, since the blockade error can be suppressed only when $\Omega \gg \{V_1, V_2, V_e\}$. Take the analysis leading to Fig. 6, for example, where $V_1, V_2, V_e \lesssim 0.36 \times 2\pi$ MHz; a two-photon Rabi frequency larger than $3 \times 2\pi$ MHz in π pulses of the protocols is preferable. This is, in principle, possible: Refs. [43] and [44] reported coherent GHz-rate Rabi oscillations between ground and $nS_{1/2}$ Rydberg states with $n \geq 30$ via laser pulses of nanosecond duration on a rubidium (cesium) vapor. For single cold atoms, π pulses at a Rabi frequency of $7 \times 2\pi$ MHz between ground and $58d_{3/2}$ states of ^{87}Rb were used in Ref. [45]. Since the Rydberg states in our example are relatively high, we assume that a Rabi frequency of $\Omega/2\pi = 5$ MHz can be easily realized for a conservative estimate. With such an Ω , we find that $1 - \mathcal{F}$ in Fig. 6(a) [Fig. 6(b)] increases by 6×10^{-3} [32×10^{-3}].

Stable laser sources are also required to achieve the predicted gate performance in Fig. 6. Our protocols require the establishment of the superposition states defined in Eq. (5), whose preparation depends on correctly setting the magnitude and phase of the laser fields in Fig. 2, provided that the laser frequency is stable enough [46,47]. We take Protocol I as an example to estimate the precision necessary for the parameters of the laser fields to reach the gate fidelity in

Fig. 6. If the phase from the dipole matrix element is fixed to be 0, then β_0 in Eq. (3) is determined by the phases of the laser fields. Suppose the relative fluctuations of the laser phase and the laser Rabi frequency are bounded by ζ_1 and $|\delta\Omega_k/\Omega_k| \leq \zeta_2$; then the phase term β_0 and interaction coefficients V_1 , V_2 , and V_e in Eqs. (3) and (6) have relative errors of up to $2\zeta_1$ and $2\zeta_2$, respectively, leading to relative errors of $2\zeta_1$ for ϕ and $2\zeta_2$ for $\pi - \alpha$ and θ in Eq. (11) of Protocol I. Furthermore, incorrect laser Rabi frequency and timing also impact the accuracy of the Rabi pulse area, resulting in population leakage to Rydberg states unless their added effects cancel. During pulses 1 and 2 in Protocol I, the population transfer errors are about $(\pi\delta\Omega_k/2\Omega_k)^2$ and $(\pi\delta t/2t)^2$ for incorrect Rabi frequencies and timing in a pulse duration of t , respectively. Because $(\pi\delta\Omega_k/2\Omega_k)^2 \sim \zeta_2^2$, the latter errors are negligible compared with those of the angles $\pi - \alpha$ and θ . As a consequence, one needs the fluctuations of the laser phase and electric field bounded by $|\delta\beta_0/\beta_0| + |\delta\Omega_k/\Omega_k| \lesssim 10^{-3}$ to achieve the gate fidelity predicted in Fig. 6. The phase fluctuation of laser beams can be made much smaller than 10^{-3} [39,48], but the intensity fluctuation of the lasers was several percent in typical experiments on Rydberg quantum gates [45,49]. Nevertheless, lasers with root-mean-square intensity noise of less than 0.1% were recently realized in the preparation of Rydberg states of ^{39}K [50], indicating the possibility of realizing high-fidelity Barenco gates in the near future. Alternatively, numerical simulation in [51] showed that optimal control may be used to identify pulse sequences that are inherently robust to fluctuations of Rabi frequencies. Nevertheless, it is an open problem to implement these techniques in our Barenco gates to realize the gate performance in Fig. 6.

Severe atom loss during the gate sequence is another issue in current Rydberg gate experiments [21,22,49,52–54], and such loss may be from unwanted couplings that result in populating Rydberg states other than the targeted ones [22]. One possibility leading to unwanted couplings is level mixing due to stray electric fields [33,55], which can be suppressed by microwave-induced dressing of Rydberg states [56]. Another possibility is multiple cycles of rise and fall of optical lasers [22], a problem that may be partly avoided by exploiting gates that use only one pulse for qubit entanglement [32,57–59].

VI. CONCLUSIONS

In conclusion, we propose two protocols to realize a universal quantum gate \mathbb{B} based on a tunable noncollinear interaction of the form $V|r_1r_2\rangle\langle r_1r_3| + \text{H.c.}$ We show that this noncollinear interaction is achievable for a quantum system that exhibits a usual blockade interaction of the form $\sum_{j,k} b_{jk}|R_jR_k\rangle\langle R_jR_k|$, such as Coulomb blockade in quantum dots or Rydberg blockade in neutral atoms. Among the three angles α , θ , and ϕ in \mathbb{B} , ϕ is freely tunable via adjustment of the phases of external fields in the first protocol, while the other two angles in the first protocol and all three angles in the second protocol can be tuned by adjusting the interaction coefficients and wait durations. In particular, the first protocol can also lead to CNOT and controlled-Y gates. Analyses of the gate protocols using Rydberg interaction in neutral atoms

show that the gate operation time can be in the microsecond regime with an intrinsic fidelity error of the order of 10^{-3} . Such an intrinsic fidelity, however, is achievable only if technical problems do not occur, which is an open problem at the moment.

ACKNOWLEDGMENTS

The author thanks Yan Lu for fruitful discussions and acknowledges support from the Fundamental Research Funds for the Central Universities and the 111 Project (B17035).

APPENDIX A: INTERACTIONS IN THE EXAMPLE OF \mathbb{B} WITH NEUTRAL ATOMS

We consider two-photon transitions from ground states to Rydberg states via the intermediate hyperfine level $|5p_{1/2}, F=1, m_F=1\rangle$ and choose $(n_1, n_2) = (96, 102)$. Then the vdWI coefficients are [29] $C_6(|R_0 R_1\rangle) = 35.71 \times 2\pi$ THz μm^6 and $C_6(|R_0 R_2\rangle) = -10.07 \times 2\pi$ THz μm^6 . There is an exchange interaction between $|R_0 R_2\rangle$ and $|R_2 R_0\rangle$ with a tiny vdWI coefficient, $C'_6 = -5 \times 2\pi$ GHz μm^6 , which can be neglected. The character of the interaction transfers between resonant dipole-dipole interaction and vdWI at about $5 \mu\text{m}$. We choose a two-atom distance of $l = 20 \mu\text{m}$ to guarantee a picture of vdWI. Then $\{b_{01}, b_{02}\} = \{0.558, -0.157\} \times 2\pi$ MHz, and we have the following interaction strengths in units of 2π kHz,

$$\begin{aligned} V_1 &= 558 \cos^2 \beta_1 - 157 \sin^2 \beta_1, \\ V_2 &= 558 \sin^2 \beta_1 - 157 \cos^2 \beta_1, \\ V_e &= 715 \sin \beta_1 \cos \beta_1. \end{aligned}$$

APPENDIX B: GATE FIDELITY ERROR

The excited states of atoms can experience decay, the Rabi frequency Ω is not infinitely large compared with the blockade $V_{1(2)}$, and there can be population leakage out of the computational basis. The force between the two atoms can also induce drift of the atomic spacing. When the atoms are captured by optical dipole traps before and after the gate sequence, the distance between the two atoms can vary from the ideal l . These several factors cause errors in the gate operation. We denote an input state by a wave function $|\Psi_{\text{in}}\rangle$ and the output state by a density matrix ρ_{out} , which can be different from $\mathbb{B}|\Psi_{\text{in}}\rangle\langle\Psi_{\text{in}}|\mathbb{B}^\dagger$. Then the fidelity of the gate can be defined as

$$\mathcal{F} = \overline{\langle\Psi_{\text{in}}|\mathbb{B}^\dagger\rho_{\text{out}}\mathbb{B}|\Psi_{\text{in}}\rangle},$$

where the overbar means an average over all possible input states. Take Protocol I as an example; the Rydberg state decay, finiteness of Ω , and population leakage lead to errors that can

be, respectively, approximated by [30,39]

$$\begin{aligned} E_{\text{de}} &= \frac{(\frac{\pi}{\Omega} + T)(\tau_1 + \tau_2)/2}{\tau_1 \tau_2 + \sin^2 \beta_1 \cos^2 \beta_1 (\tau_1 - \tau_2)^2} + \left(\frac{\pi}{2\Omega} + T/2\right)/\tau_1, \\ E_{\text{bl}} &= 2 \frac{V_1^2 + V_2^2}{\Omega^2}, \\ E_{\text{le}} &= \frac{\Omega^2}{\Delta_1^2} + \frac{\Omega^2}{2\Delta_2^2}, \end{aligned}$$

where τ_j is the lifetime of state $|R_j\rangle$, $j = 1, 2$. Here, $\Delta_{1(2)}/2\pi = 1.8(1.5)$ GHz is the detuning for the dominant leakage channel. For example, the level nearest to $|R_0\rangle$ that can be transferred from the $5p_{1/2}$ state is $|94d_{3/2}, m_J = 1/2, m_l = 3/2\rangle$, with a detuning of $\Delta_1/2\pi = 1.8$ GHz.

During the wait periods, because both atoms are in Rydberg states, entanglement between motional states and internal states may arise. This effect, however, is negligible. For example, if two atoms are in the state $|R_0 R_1\rangle = |R_1 R_1\rangle$, a force $-6C_6(|R_0 R_1\rangle)/l^7$ arises. With this force, the relative speed between the two atoms changes by $|\delta v| = 6C_6(|R_0 R_1\rangle)T_{\text{Ry}}/\mu l^7$, where μ is the mass of the atom and T_{Ry} is the time for which the atoms are in the Rydberg states. For $T_{\text{Ry}} = 1 \mu\text{s}$ and $l = 20 \mu\text{m}$, we have $\delta v = 7.6 \times 10^{-4}$ m/s. If the initial relative speed is 0, the two-atom separation will change by about $3.8 \times 10^{-4} \mu\text{m}$ after one gate cycle, which is negligible compared with l .

For gate fidelity errors caused by distance fluctuation of the atoms, we note that the parameters characterizing a trap include the trap depth U , the oscillation frequencies $\{\omega_x, \omega_y, \omega_z\}$, and the averaged variances of the position $\{\sigma_x^2, \sigma_y^2, \sigma_z^2\}$. We consider the case where the motional state of a trapped neutral atom is thermal, i.e., $k_B T_a/2 \geq \hbar\omega_j$, $j = x, y, z$, where k_B is the Boltzmann constant and T_a is the effective temperature of atoms. For an optical tweezer created by a single laser beam of wavelength λ and waist w that propagates along z , we have $\sigma_x^2 = \sigma_y^2 = \frac{w^2 T_a}{4 U}$, $\sigma_z^2 = \xi^2 \sigma_x^2$, $\xi = \sqrt{2\pi} w/\lambda$, where U and ξ are the potential depth and anisotropy factor of the trap, respectively [39]. The position distributions of the two qubits depend on $\{\sigma_x^2, \sigma_y^2, \sigma_z^2\}$. In different runs of the gate, the fluctuation of the atomic location adds an extra error $\overline{E}_{\mathcal{L}}$ to the total gate fidelity error, which can be numerically evaluated by Monte Carlo integration [30]. For $\{w, \lambda\} = \{3.0, 1.1\} \mu\text{m}$, $T = 0.5 \mu\text{s}$, and $U = 20$ mK, numerical calculation shows that it is in the interval of $[1.4, 52][1.0, 49] \times 10^{-4}$ for Protocol I (Protocol II) when $T_a \in [10, 200] \mu\text{K}$. We also considered a similar setup analyzed in Ref. [40], but with atoms cooled to motional ground states, and analyzed $\overline{E}_{\mathcal{L}}$ as a function of the trap depth U . Numerical calculation shows that $\overline{E}_{\mathcal{L}} < 7 \times 10^{-5}$ for both protocols when $U > 1 \mu\text{K}$. These analyses mean that one can suppress the error caused by position fluctuation through laser cooling of atoms.

- [1] M. A. Nielsen and I. L. Chuang, in *Quantum Computation and Quantum Information* (Cambridge University Press, Cambridge, UK, 2000).
- [2] C. P. Williams, *Explorations in Quantum Computing*, 2nd ed. *Texts in Computer Science*, edited by D. Gries and F. B. Schneider (Springer-Verlag, London, 2011).

- [3] D. Deutsch, Quantum computational networks, *Proc. R. Soc. Lond. A* **425**, 73 (1989).
- [4] A. Barenco, A universal two-bit gate for quantum computation, *Proc. R. Soc. Lond. A* **449**, 679 (1995).
- [5] T. Sleator and H. Weinfurter, Realizable Universal Quantum Logic Gates, *Phys. Rev. Lett.* **74**, 4087 (1995).

- [6] D. P. DiVincenzo, Two-bit gates are universal for quantum computation, *Phys. Rev. A* **51**, 1015 (1995).
- [7] D. Loss and D. P. DiVincenzo, Quantum computation with quantum dots, *Phys. Rev. A* **57**, 120 (1998).
- [8] S.-L. Zhu and Z. D. Wang, Implementation of Universal Quantum Gates Based on Nonadiabatic Geometric Phases, *Phys. Rev. Lett.* **89**, 097902 (2002).
- [9] M. J. Bremner, C. M. Dawson, J. L. Dodd, A. Gilchrist, A. W. Harrow, D. Mortimer, M. A. Nielsen, and T. J. Osborne, Practical Scheme for Quantum Computation with any Two-Qubit Entangling Gate, *Phys. Rev. Lett.* **89**, 247902 (2002).
- [10] S. Bravyi and A. Kitaev, Universal quantum computation with ideal Clifford gates and noisy ancillas, *Phys. Rev. A* **71**, 022316 (2005).
- [11] R. Hanson and G. Burkard, Universal Set of Quantum Gates for Double-Dot Spin Qubits with Fixed Interdot Coupling, *Phys. Rev. Lett.* **98**, 050502 (2007).
- [12] E. Zahedinejad, J. Ghosh, and B. C. Sanders, High-Fidelity Single-Shot Toffoli Gate via Quantum Control, *Phys. Rev. Lett.* **114**, 200502 (2015).
- [13] A. Sawicki and K. Karnas, Criteria for universality of quantum gates, *Phys. Rev. A* **95**, 062303 (2017).
- [14] S. Puri, P. L. McMahon, and Y. Yamamoto, Universal logic gates for quantum-dot electron-spin qubits using trapped quantum-well exciton polaritons, *Phys. Rev. B* **95**, 125410 (2017).
- [15] C. Monroe, D. M. Meekhof, B. E. King, W. M. Itano, and D. J. Wineland, Demonstration of a Fundamental Quantum Logic Gate, *Phys. Rev. Lett.* **75**, 4714 (1995).
- [16] G. J. Pryde, A. G. White, T. C. Ralph, and D. Branning, Demonstration of an all-optical quantum controlled-NOT gate, *Nature* **426**, 264 (2003).
- [17] M. Veldhorst, C. H. Yang, J. C. C. Hwang, W. Huang, J. P. Dehollain, J. T. Muhonen, S. Simmons, A. Laucht, F. E. Hudson, K. M. Itoh, A. Morello, and A. S. Dzurak, A two qubit logic gate in silicon, *Nature* **526**, 410 (2015).
- [18] J. M. Chow, J. M. Gambetta, A. D. Córcoles, S. T. Merkel, J. A. Smolin, C. Rigetti, S. Poletto, G. A. Keefe, M. B. Rothwell, J. R. Rozen, M. B. Ketchen, and M. Steffen, Universal Quantum Gate set Approaching Fault-Tolerant Thresholds with Superconducting Qubits, *Phys. Rev. Lett.* **109**, 060501 (2012).
- [19] R. Barends, J. Kelly, A. Megrant, A. Veitia, D. Sank, E. Jeffrey, T. C. White, J. Mutus, A. G. Fowler, B. Campbell, Y. Chen, Z. Chen, B. Chiaro, A. Dunsworth, C. Neill, P. O'Malley, P. Roushan, A. Vainsencher, J. Wenner, A. N. Korotkov, A. N. Cleland, and J. M. Martinis, Superconducting quantum circuits at the surface code threshold for fault tolerance, *Nature (London)* **508**, 500 (2014).
- [20] C. J. Ballance, T. P. Harty, N. M. Linke, M. A. Sepiol, and D. M. Lucas, High-Fidelity Quantum Logic Gates using Trapped-ion Hyperfine Qubits, *Phys. Rev. Lett.* **117**, 060504 (2016).
- [21] L. Isenhower, E. Urban, X. L. Zhang, A. T. Gill, T. Henage, T. A. Johnson, T. G. Walker, and M. Saffman, Demonstration of A Neutral Atom Controlled-NOT Quantum Gate, *Phys. Rev. Lett.* **104**, 010503 (2010).
- [22] K. M. Maller, M. T. Lichtman, T. Xia, Y. Sun, M. J. Piotrowicz, A. W. Carr, L. Isenhower, and M. Saffman, Rydberg-blockade controlled-not gate and entanglement in a two-dimensional array of neutral-atom qubits, *Phys. Rev. A* **92**, 022336 (2015).
- [23] T. F. Gallagher, *Rydberg Atoms* (Cambridge University Press, Cambridge, UK, 2005).
- [24] R. Hanson, L. P. Kouwenhoven, J. R. Petta, S. Tarucha, and L. M. K. Vandersypen, Spins in few-electron quantum dots, *Rev. Mod. Phys.* **79**, 1217 (2007).
- [25] J. Q. You and F. Nori, Superconducting circuits and quantum information, *Phys. Today* **58**(11), 42 (2005).
- [26] M. Saffman, T. G. Walker, and K. Mølmer, Quantum information with Rydberg atoms, *Rev. Mod. Phys.* **82**, 2313 (2010).
- [27] X. Xu, W. Yao, B. Sun, D. G. Steel, A. S. Bracker, D. Gammon, and L. J. Sham, Optically controlled locking of the nuclear field via coherent dark-state spectroscopy, *Nature* **459**, 1105 (2009).
- [28] O. Ávalos-Ovando, D. Mastrogiuseppe, and S. E. Ulloa, Non-collinear exchange interaction in transition metal dichalcogenide edges, *Phys. Rev. B* **93**, 161404 (2016).
- [29] X.-F. Shi, F. Bariani, and T. A. B. Kennedy, Entanglement of neutral-atom chains by spin-exchange Rydberg interaction, *Phys. Rev. A* **90**, 062327 (2014).
- [30] X.-F. Shi and T. A. B. Kennedy, Annulled van der Waals interaction and fast Rydberg quantum gates, *Phys. Rev. A* **95**, 043429 (2017).
- [31] Y. O. Dudin and A. Kuzmich, Strongly interacting Rydberg excitations of a cold atomic gas, *Science* **336**, 887 (2012).
- [32] D. Jaksch, J. I. Cirac, P. Zoller, S. L. Rolston, R. Côté, and M. D. Lukin, Fast Quantum Gates for Neutral Atoms, *Phys. Rev. Lett.* **85**, 2208 (2000).
- [33] M. Saffman, Quantum computing with atomic qubits and Rydberg interactions: Progress and challenges, *J. Phys. B* **49**, 202001 (2016).
- [34] J. D. Thompson, T. L. Nicholson, Q.-Y. Liang, S. H. Cantu, A. V. Venkatramani, S. Choi, I. A. Fedorov, D. Viscor, T. Pohl, M. D. Lukin, and V. Vuletić, Symmetry-protected collisions between strongly interacting photons, *Nature* **542**, 206 (2017).
- [35] I. I. Beterov, M. Saffman, E. A. Yakshina, D. B. Tretyakov, V. M. Entin, S. Bergamini, E. A. Kuznetsova, and I. I. Ryabtsev, Two-qubit gates using adiabatic passage of the Stark-tuned Forster resonances in Rydberg atoms, *Phys. Rev. A* **94**, 062307 (2016).
- [36] D. Petrosyan, F. Motzoi, M. Saffman, and K. Mølmer, High-fidelity Rydberg quantum gate via a two-atom dark state, *Phys. Rev. A* **96**, 042306 (2017).
- [37] X.-F. Shi, P. Svetlichnyy, and T. A. B. Kennedy, Spin-charge separation of dark-state polaritons in a Rydberg medium, *J. Phys. B* **49**, 074005 (2016).
- [38] J. F. Poyatos, J. I. Cirac, and P. Zoller, Complete Characterization of a Quantum Process: The Two-Bit Quantum Gate, *Phys. Rev. Lett.* **78**, 390 (1997).
- [39] M. Saffman and T. G. Walker, Analysis of a quantum logic device based on dipole-dipole interactions of optically trapped Rydberg atoms, *Phys. Rev. A* **72**, 022347 (2005).
- [40] X.-F. Shi, Rydberg Quantum Gates Free from Blockade Error, *Phys. Rev. Appl.* **7**, 064017 (2017).
- [41] L. S. Theis, F. Motzoi, F. K. Wilhelm, and M. Saffman, High-fidelity Rydberg-blockade entangling gate using shaped, analytic pulses, *Phys. Rev. A* **94**, 032306 (2016).
- [42] J. Ghosh, S. N. Coppersmith, and M. Friesen, Pulse sequences for suppressing leakage in single-qubit gate operations, *Phys. Rev. B* **95**, 241307 (2017).

- [43] B. Huber, T. Baluksian, M. Schlagmüller, A. Kölle, H. Kübler, R. Löw, and T. Pfau, GHz Rabi Flopping to Rydberg States in Hot Atomic Vapor Cells, *Phys. Rev. Lett.* **107**, 243001 (2011).
- [44] A. Urvoy, F. Ripka, I. Lesanovsky, D. Booth, J. P. Shaffer, T. Pfau, and R. Löw, Strongly Correlated Growth of Rydberg Aggregates in a Vapor Cell, *Phys. Rev. Lett.* **114**, 203002 (2015).
- [45] A. Gaëtan, Y. Miroshnychenko, T. Wilk, A. Chotia, M. Viteau, D. Comparat, P. Pillet, A. Browaeys, and P. Grangier, Observation of collective excitation of two individual atoms in the Rydberg blockade regime, *Nat. Phys.* **5**, 115 (2009).
- [46] J. de Hond, N. Cisternas, G. Lochead, and N. J. van Druten, A medium-finesse optical cavity for the stabilization of Rydberg lasers, *Appl. Opt.* **56**, 5436 (2017).
- [47] R. Legaie, C. J. Picken, and J. D. Pritchard, Sub-Khz Excitation Lasers for Quantum Information Processing with Rydberg Atoms [arXiv:1711.02645](https://arxiv.org/abs/1711.02645).
- [48] D. J. Wineland, C. Monroe, W. M. Itano, D. Leibfried, B. E. King, and D. M. Meekhof, Experimental issues in coherent quantum-state manipulation of trapped atomic ions, *J. Res. Natl. Inst. Stand. Technol.* **103**, 259 (1998).
- [49] T. Wilk, A. Gaëtan, C. Evellin, J. Wolters, Y. Miroshnychenko, P. Grangier, and A. Browaeys, Entanglement of Two Individual Neutral Atoms using Rydberg Blockade, *Phys. Rev. Lett.* **104**, 010502 (2010).
- [50] A. Arias, S. Helmrich, C. Schweiger, L. Ardizzone, G. Lochead, and S. Whitlock, Versatile, high-power 460nm laser system for Rydberg excitation of ultracold potassium, *Opt. Express* **25**, 14829 (2017).
- [51] M. H. Goerz, E. J. Halperin, J. M. Aytac, C. P. Koch, and K. B. Whaley, Robustness of high-fidelity Rydberg gates with single-site addressability, *Phys. Rev. A* **90**, 032329 (2014).
- [52] X. L. Zhang, L. Isenhower, A. T. Gill, T. G. Walker, and M. Saffman, Deterministic entanglement of two neutral atoms via Rydberg blockade, *Phys. Rev. A* **82**, 030306 (2010).
- [53] Y.-Y. Jau, A. M. Hankin, T. Keating, I. H. Deutsch, and G. W. Biedermann, Entangling atomic spins with a Rydberg-dressed spin-flip blockade, *Nat. Phys.* **12**, 71 (2016).
- [54] Y. Zeng, P. Xu, X. He, Y. Liu, M. Liu, J. Wang, D. J. Papoular, G. V. Shlyapnikov, and M. Zhan, Entangling Two Individual Atoms of Different Isotopes via Rydberg Blockade, *Phys. Rev. Lett.* **119**, 160502 (2017).
- [55] D. S. Weiss and M. Saffman, Quantum computing with neutral atoms, *Phys. Today* **70**(7), 44 (2017).
- [56] D. W. Booth, J. Isaacs, and M. Saffman, Reducing the sensitivity of Rydberg atoms to dc electric fields using two-frequency ac field dressing, *Phys. Rev. A* **97**, 012515 (2018).
- [57] R. Han, H. K. Ng, and B.-G. Englert, Implementing a neutral-atom controlled-phase gate with a single Rydberg pulse, *Europhys. Lett.* **113**, 40001 (2016).
- [58] S.-L. Su, E. Liang, S. Zhang, J.-J. Wen, L.-L. Sun, Z. Jin, and A.-D. Zhu, One-step implementation of the Rydberg-Rydberg-interaction gate, *Phys. Rev. A* **93**, 012306 (2016).
- [59] S.-L. Su, Y. Tian, H. Z. Shen, H. Zang, E. Liang, and S. Zhang, Applications of the modified Rydberg antiblockade regime with simultaneous driving, *Phys. Rev. A* **96**, 042335 (2017).